Rare Metal Materials and Engineering
Volume 48, Issue 5, May 2019
Available online at www.rmme.ac.cn

Science Press

Cite this article as: Rare Metal Materials and Engineering, 2019, 48(5): 1421-1428.

ARTICLE

Effects of SiC and Al_2O_3 Particles on Micro-abrasion Behavior of Ti-25Nb-3Mo-3Zr-2Sn Alloy

Wang Zhenguo[1], Bi Yanze[1], Li Yan[1], Cai Haijiao[2]

[1] Beihang University, Beijing 100191, China; [2]GRIMED Medical (Beijing) Co., Ltd, Beijing 102200, China

Abstract: The effects of SiC and Al_2O_3 abrasive particles on micro-abrasion behavior of a biomaterial Ti-25Nb-3Mo-3Zr-2Sn alloy in Hank's solution was investigated. The effects of particle size and type were considered. The specific wear rate, friction coefficient, wear mechanism and the synergistic effect between the micro-abrasion and corrosion were studied. The results show that the specific wear rates increase with increasing of the particle size. Since the hardness and machinability of SiC particle is higher, the material loss caused by the SiC particle is greater than that of the Al_2O_3 particle with the same size. The average friction coefficients obtained in Hank's solution are larger than those in distilled water for the SiC particle; however, the Al_2O_3 particle is just the opposite. For the same particle size, the average friction coefficients acquired by the Al_2O_3 particle is larger than that by the SiC particle. Due to the corrosivity of Hank's solution, the stability of the friction coefficient in Hank's solution is poor compared to that of distilled water. With a decrease of the particle size, the wear mechanism changes from a three-body rolling abrasion to a mixed mode and finally to a two-body grooving abrasion. The mechanistic map of the *AC-PA* against the *PA* illustrates that the contribution of corrosion to the total material loss cannot be ignored, and the main regime is abrasion-corrosion.

Key words: micro-abrasion; abrasive particles; biomaterial; Ti-25Nb-3Mo-3Zr-2Sn; synergistic effect

As a new metastable β titanium alloy suitable for biomedical applications, the TLM alloy with a nominal chemical composition of Ti-25Nb-3Mo-3Zr-2Sn (wt%) has been developed[1,2]. The TLM alloy consists of the non-toxic alloying elements Mo, Nb, Zr and Sn and shows low elastic modulus, excellent strength and toughness, remarkable shape memory, good biocompatibility and osteoconduction[1-6]. These properties make TLM alloy ideal for wide use in biomedical applications, such as implants for bone and joint replacements as well as orthodontic arch wires and stents[2, 3]. Intensive investigations have focused on the alloy, such as phase transformation and microstructure[1, 4], mechanical properties[1, 2], osteoblast response[6], biocompatibility[3, 7] and corrosion resistance[8]. However, little research has been conducted on the wear behavior of the TLM alloy in a human body environment, especially the micro-abrasion behavior. The present author and others have studied the effect of the friction pairs on micro-scale abrasive wear behavior and the interaction between wear and corrosion for the alloy in simulated body fluids[9-12].

During the micro-scale abrasive wear process, the influence of the abrasive particles is important, because the wear debris generated during the wear process leads to osteolysis and aseptic loosening and is the major cause of artificial joint failure[13]. Therefore, some researchers have studied the effect of these particles on the micro-scale abrasive wear behavior of implant materials. Silicon carbide (SiC), alumina (Al_2O_3) and diamond are widely used as the abrasive particles in these study[14-17]. Research of Shipway et al.[14] showed that the relative wear rates of the materials depended strongly upon the abrasive particle type selected and the hardness of abrasive particles has an important influence on wear mechanisms. Suner et al.[15] noted that a reduction in the particle size can significantly affect the abra-

Received date: May 15, 2018
Foundation item: National Natural Science Foundation of China (51401027); China Postdoctoral Science Foundation Funded Project (2016M591040)
Corresponding author: Li Yan, Ph. D., Professor, School of Materials Science and Engineering, Beihang University, Beijing 100191, P. R. China, Tel: 0086-10-82315989, E-mail: liyan@buaa.edu.cn

sion-corrosion wear mechanisms and the wear-induced corrosion response of the CoCrMo alloy. The abrasive particle size also plays an important role in the micro-abrasion process[16-19]. Thakare et al.[20] noted that the sharp rise in wear rates associated with the transition from ductile is due to the plastic deformation-dominated material removal progressing to a more fracture-related material removal as the particle size increases. Some authors contend that the abrasive concentration also plays an important role in the micro-abrasion[20-22]. Micro-abrasion-corrosion experiments on a titanium alloy in Hank's solution by Stack et al.[22] indicated that the wear rate is dependent on load and particle concentration. Telfer et al.[23] revealed that the effect of particle concentration within various slurries and the active dissolution region increased the erosion rate due to an increase in concentration. Cozza[24] showed that the coefficient of friction behavior is independent of the normal force in both the concentrations of abrasive slurries.

To better understand the effect of particle style and size on the micro-abrasion behavior of the TLM alloy, the objective of this work was to investigate the specific wear rate, friction coefficient, wear mechanism and synergistic effect between the micro-abrasion and corrosion of the biomaterial Ti-25Nb-3Mo-3Zr-2Sn alloy.

1 Experiment

1.1 Sample preparation

The Ti-25Nb-3Mo-3Zr-2Sn (TLM) alloy was the target material, provided by the Northwest Institute for Nonferrous Metal Research, China, and received as a rolled plate with 3.2 mm thickness. The chemical composition of the alloy is presented in Table 1. The test samples (33 mm ×25 mm ×3 mm) were taken from the plate by wire-electrode cutting. The samples were heat-treated in solution at 760 °C for 60 min, followed by air cooling, and then aged at 550 °C for 360 min, followed by air cooling in a box furnace. The samples were gradually ground with waterproof SiC paper at 200#, 400#, 600#, 800#, 1000#, 1200# and 1500#, then cleaned ultrasonically in alcohol and distilled water for 10 min separately and dried with a cold air stream from an electric hair dryer. The microstructure of the test sample is shown in Fig.1. It primarily consists of β-phase and fine acicular α precipitates.

1.2 Abrasive particles

For the abrasive particles, the two different materials SiC and Al_2O_3 were employed, and the typical hardnesses are 21000~26000 and 18000~20000 MPa for SiC and Al_2O_3, respectively. For simulation of the human body environment, small grain abrasive particle sizes were chosen. They were purchased from the same provider.

The following three different SiC particles were used in micro-abrasion wear tests: SiC F1000 (classified by the Federation of European Producers of Abrasives), with an average particle size of (4.5±0.8) μm standard deviation; SiC F1200, with an average particle size of (3.0±0.5) μm standard deviation; and SiC F2000, with an average grain size of (1.5±0.5) μm standard deviation. For comparison, a study of the effect of Al_2O_3 F1200 particle was also conducted. SEM topographies of these particles are presented in Fig.2.

Table 1 Chemical composition of TLM alloy (wt%)

Ti	Nb	Mo	Sn	Zr	C	N	H	O
Bal.	25.1	2.90	2.02	3.08	0.01	0.03	0.003	0.004

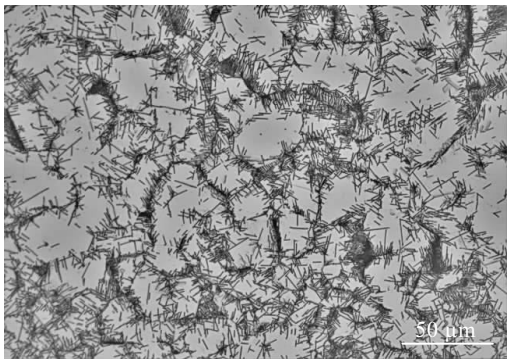

Fig.1 Optical microstructure of the TLM alloy after heat treatment

1.3 Micro-abrasion tests

Micro-abrasion tests were performed using a TE-66 Micro-Scale Abrasion Tester (Phoenix, UK). A Si_3N_4 ball with 25.4 mm in diameter was rotated against samples in the presence of a slurry of particles. The Si_3N_4 ball was supplied by Shanghai United Technology Co. Ltd, and the properties are listed in Table 2.

In the tests, the temperature was maintained at (37± 0.5) ℃, the particle concentration was 0.2 g/cm^3, the applied load was 2.0 N, the sliding speed was 50 r/min, and the sliding distance was 89.73 m. The liquid medium was Hank's solution[8] and distilled water, and the pH value (7.4±0.1) was adjusted with an acid-base balance fluid. The overall test matrix is detailed in Table 3.

To maintain the uniformity of slurry concentration and the consistency of test temperature, a digital, high-powered, speed-controlled DF-101S magnetic stirrer was used with a constant heating temperature and a single head stirrer. All tests were conducted without interruption, and the abrasive slurry was continuously agitated and fed between the Si_3N_4 ball and the samples with a peristaltic pump.

1.4 Analytical methods

A JSM-6460LV scanning electron microscope (SEM) was used to observe the worn surface morphologies. A calibrated digital optical microscope (OM, 15JE) was employed to measure the diameter of the wear scars, b, which was used to calculate the wear volume V (Eq.(1))[9].

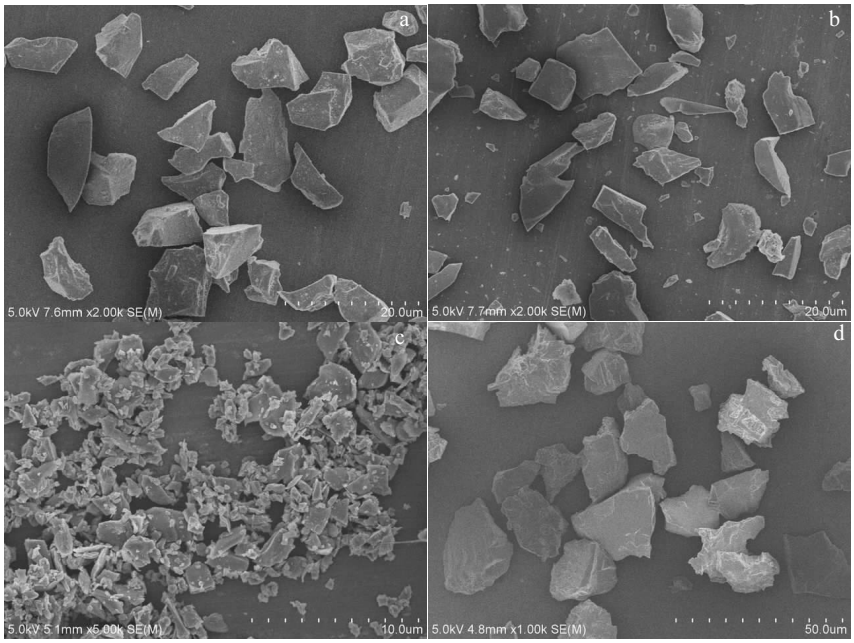

Fig.2 SEM topographies of different abrasive particles: (a) SiC F1000, (b) SiC F1200, (c) SiC F2000, and (d) Al_2O_3 F1200

Table 2 Physical properties of Si_3N_4 ceramic ball

Density/ g·cm^{-3}	Thermal expansion coefficient/K^{-1}	Poisson's ratio	Hard-ness/MPa	Elasticity modulus/GPa
3.25	3.2×10^{-6}	0.26	15000	310

Table 3 Test conditions during micro-scale abrasion testing

Parameter	conditions
Load/ N	2.0
Abrasive concentration/ g·cm^{-3}	0.2
sliding speed/r·min^{-1}	50
sliding distances/m	89.73
liquid medium	Hank's solution and distilled water
liquid temperature/℃	37±0.5
Liquid pH	7.4±0.1
Counterface material	Si_3N_4 ceramic ball (with 25.4 mm in diameter)

$$V = \frac{\pi b^4}{64R} \quad \text{for } b << R \tag{1}$$

where V and b are the wear volume and diameter of the wear scar, respectively. The value of R was 25.4 mm.

The specific wear rate, k, was estimated by dividing the wear volume from Eq.(1) by the applied load (N) and total sliding distance (L, 89.73 m), see Eq.(2)[23].

$$k = V/LN \tag{2}$$

The synergistic effect of micro-abrasion-corrosion was computed through Eq.(3)[23].

$$S=AC-PA \tag{3}$$

where S, AC and PA are the synergistic effect, abrasion-corrosion and abrasion, respectively.

2 Results and Discussion

2.1 Specific wear rates

The results of the specific wear rates for the pure abrasion (*PA*, tested in distilled water) and micro-abrasion corrosion (*AC*, tested in Hank's solution) are shown in Fig.3 and Table 4. The specific wear rate, k, increased with an increase in particle size for both the PA and AC tests. It can also be seen that the value of k obtained from the SiC F1200 particle is greater than the value obtained from the Al_2O_3 F1200 particle. During the test process, the effect of the particle on the wear rate has many aspects including particle size, hardness, shape and type. In general, the wear rate of the metal material increased as the particle size increased, as shown in Fig.3. The three abrasive expressions of F1000, F1200 and F2000, corresponded to (4.5±0.8), (3.0±0.5) and (1.5±0.5) μm, respectively.

However, after the particle reached a critical size, the wear rate of the material no longer increased. The critical size of the particle changed with the different properties of the metal[24]. Sasada found that the influence of particle size on wear rates can be divided into three groups[25]. First, for particle sizes larger than the critical size, the wear rate did not change with the change in particle size. Second, for particle sizes between the critical size and the jump size, the wear rate decreased as the particle size decreased. Finally, for particle sizes smaller than the jump size, the wear rate was unchanged. According to these findings, the particle size was between the critical size and the jump size that was used in this study.

As mentioned in Section 1.2, the hardness of the SiC is

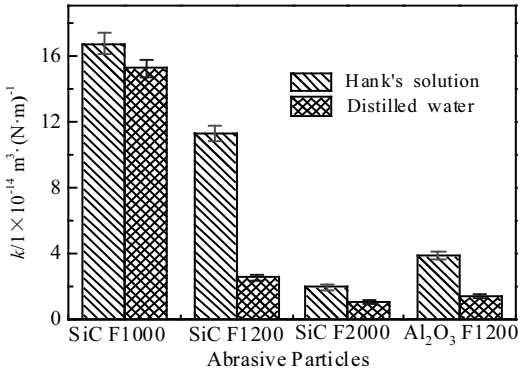

Fig.3 Wear rates of Ti-25Nb-3Mo-3Zr-2Sn alloy under different style of abrasive

Table 4 Specific wear rates vs. different abrasive particle

Abrasive	Specific wear rate, k/m^3·(N·m)$^{-1}$	
	AC	*PA*
SiC F1000	1.67×10^{-13}	1.52×10^{-13}
SiC F1200	1.13×10^{-13}	2.50×10^{-14}
SiC F2000	1.92×10^{-14}	1.01×10^{-14}
Al_2O_3 F1200	3.83×10^{-14}	1.37×10^{-14}

higher than that of the Al_2O_3 particle. Therefore, the destructive effect of the SiC is greater than that of the Al_2O_3 particle of the same size due to the higher machinability of the SiC abrasive, with wear rates shown in Fig. 3 and Table 4. The particle shape also influences the wear rate. Because of the various abrasive particle shapes, it is difficult to measure and quantify their differences, so the abrasive particle shape is qualitatively divided into three standard types[26, 27]: sharp, multiple angle and spherical, as shown in Fig.2. For sharp particles with a specific loading, when the sharp particle angle contacts the test surface, there is a serious stress concentration around the sharp angle, and the test surface of the samples is more prone to cracks, leading to more severe wear. The damage from the multiple-angle particle is more severe.

Fig. 3 also shows that the wear rates obtained in Hank's solution are greater than those in distilled water because Hank's solution contains corrosive ions such as Cl^-, $H_2PO_4^-$, HCO_3^- and SO_4^{2-} [8]. Under the simultaneous conditions of both corrosion and abrasion, the material loss affected by both factors would be accelerated, corresponding to the different wear rates, as shown in Fig.3.

2.2 Friction coefficient

Fig.4a shows the average friction coefficient of the different abrasives particle. The average values of the friction coefficient acquired in Hank's solution are larger than those in the distilled water for the SiC particle, which is just the opposite for the action of the Al_2O_3 particle. In addition, at

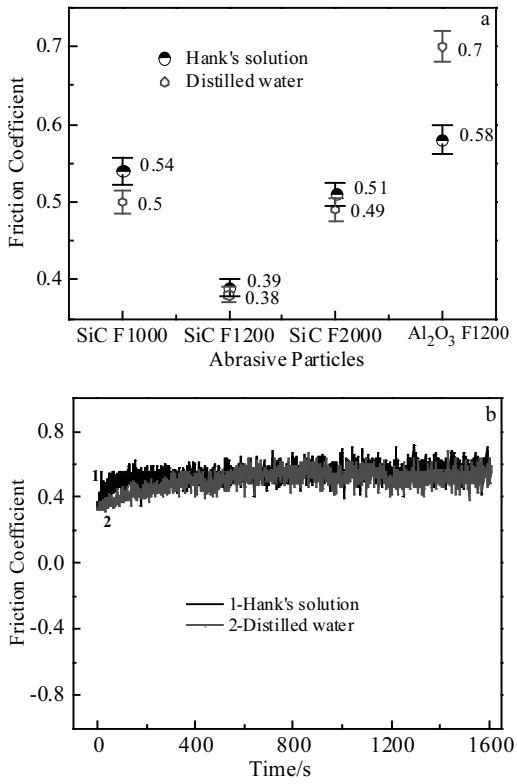

Fig.4 Friction coefficient of Ti-25Nb-3Mo-3Zr-2Sn alloy: (a) average values of COF under different style of abrasive and (b) the change of COF with time at the function of SiC F1000 abrasive

the same size (F1200), the average friction coefficient acquired by the Al_2O_3 particle is larger than that acquired by the SiC particle, due to the SiC particle having a higher level of hardness[14, 28].

The effect of the particle on friction coefficient is primarily due to its shape, size and physical properties. As mentioned above, the abrasive shapes include sharp, multiple-angle and spherical. The friction coefficient would be higher if the abrasive shape is sharp or multiple angle, resulting in a higher material loss. In addition, the friction coefficient would be affected by the surface roughness of the samples[29, 30]. It is believed that a high friction coefficient is obtained at a high roughness[30, 31]. When abrasive particles roll into the contact area, roughness peaks are detached easily compared with flat surfaces; however, this effect is only produced at the initial stage of wear test until the roughness changes[28].

Fig. 4b presents the friction coefficient as a function of the test time for the SiC F1000 particle. It was observed that the stability of the friction coefficient in Hank's solution is poor compared with that in the distilled water. During the wear process, the worn surface was exposed in the Hank's solution, which has a specific corrosivity, and the fresh worn surface was corroded and became uneven. It has been reported that

the friction coefficient is also relevant to the wear mechanisms[32], as shown in Section 2.3.

2.3 Wear morphology and mechanism

Fig. 5 shows the wear scar morphologies produced with the SiC and Al_2O_3 particles in Hank's solution. Different wear mechanisms result from the different particle sizes for the same kind particle (Fig. 5b~5f). The morphologies shown in Fig. 5a (Al_2O_3 F1200) are similar to those in Fig. 5b (SiC F1000) and Fig. 5c (SiC F1200), representing the same wear mechanism. In the middle of wear scars in Fig. 5a, Fig. 5b and Fig. 5c, the indentation morphology is leaf-like because of the accumulation of particles, as shown in Fig. 5d, and the wear mechanism is a two-body grooving wear. As shown in Fig. 5a~5c, in contrast to the leaf morphology, the rest of the area appears similarly and consists of multiple indented surfaces without directionality, indicating that three-body rolling wear was the dominant wear mechanism for the larger-sized particles, whereas the wear mechanism tends to transform to two-body grooving wear when the particle size is smaller (Fig. 5e and Fig. 5f). Moreover, as the particle size decreases, the wear mechanism changes from three-body rolling to mixed mode (rolling and grooving wear occur simultaneously) and finally to two-body grooving wear.

The wear scar morphologies produced from the micro-abrasion tests with SiC and Al_2O_3 in distilled water are shown in Fig. 6. The size of the wear scar morphologies is obviously smaller than those shown in Fig. 5. These results agree with the wear rates shown in Fig. 3. Compared with Fig. 5a, Fig. 6a shows different morphology, presenting the two-body grooving mechanism as the function of the Al_2O_3 particle, and it also shows the erosion morphology in the distilled water. The SEM images shown in Fig. 5 and Fig. 6 were induced by the abrasive wear, due to the rolling and sliding of the abrasive particles. The type of wear mechanism has a significant effect on the overall behavior of a tribological system[33]. In these figures, there is some material peeling off from the wear surface. This is because a micro-crack was produced on the wear surface during the plasticity cutting process that developed perpendicular to the sliding direction, resulting in the material peeling from the wear surface, as shown in Fig. 6a and Fig. 6b. The size of the ploughing, as shown in Fig. 5 and Fig. 6, is different for the different abrasive particles.

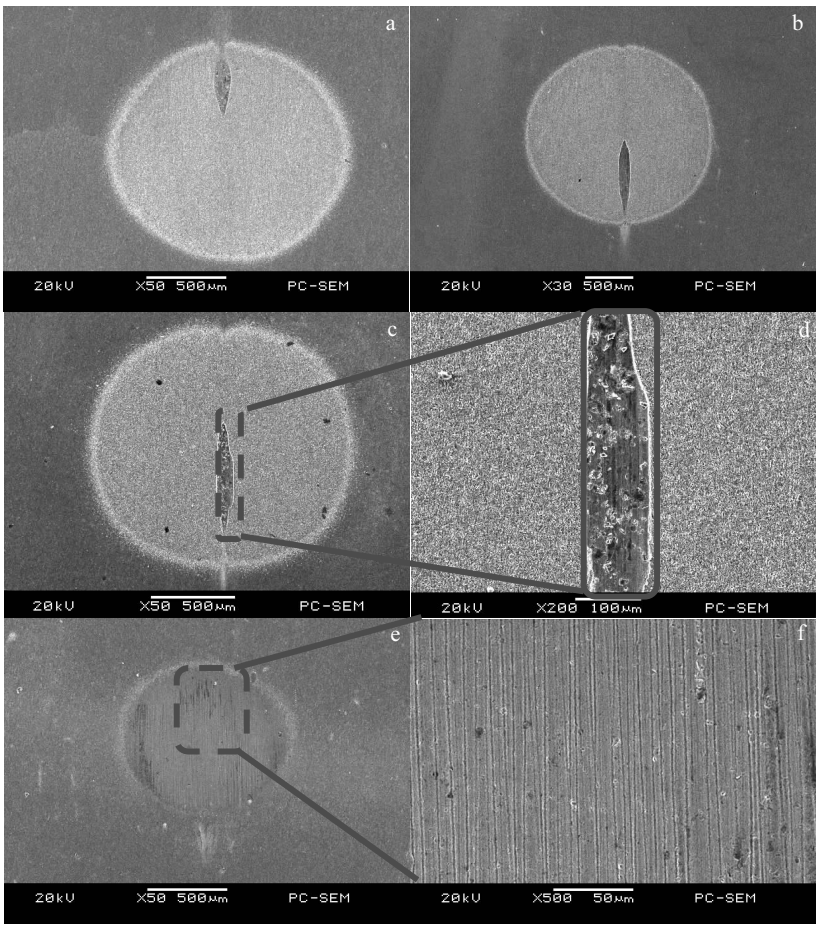

Fig.5 SEM morphologies of worn surface at different abrasive under the function of Hank's solution: (a) Al_2O_3 F1200, (b) SiC F1000, (c, d) SiC F1200, and (e, f), SiC F2000

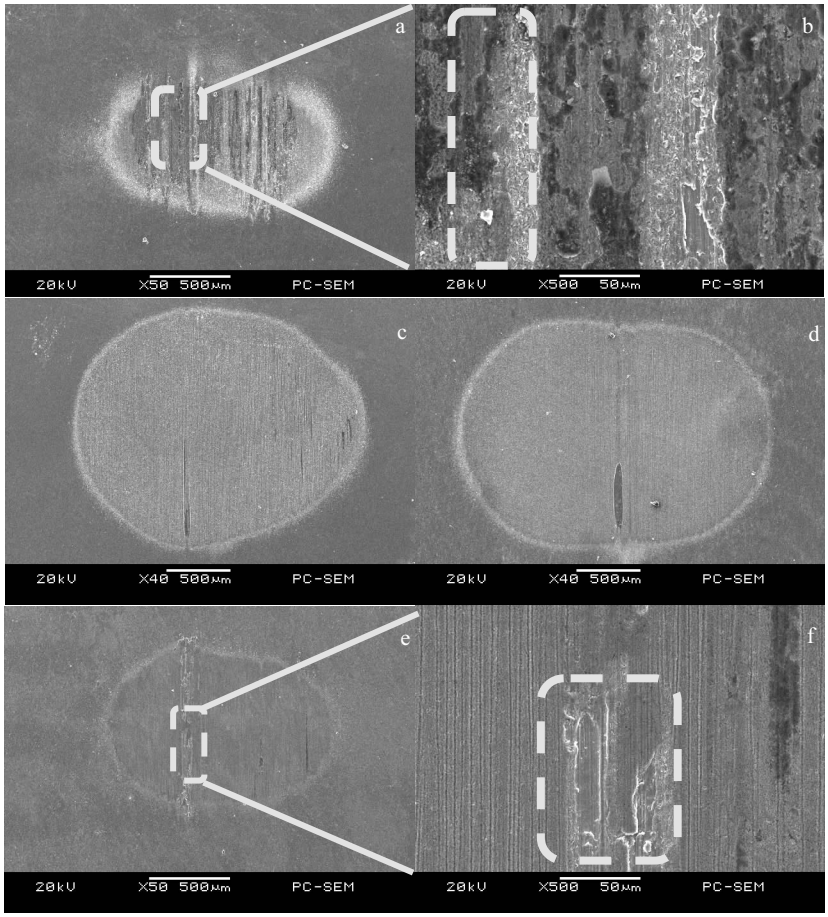

Fig.6 SEM morphologies of worn surface at different abrasive under the function of distilled water: (a, b) Al_2O_3 F1200, (c) SiC F1000, (d) SiC F1200, and (e, f) SiC F2000

Under the same load, the different sized particles caused the different shapes of ploughing. The smaller particles caused the small and shallow ploughing, as shown in Fig. 5d and Fig. 6f, which is attributed to the micro cutting and plastic deformation during the wear. It can also be seen that there are obvious pits on the wear surface, which are likely fatigue wear, as shown in Fig. 6b and Fig. 6f. In the wear-process, stress was concentrated around the hard particles such as the abrasive particles or wear debris from loading, and this compelled the surrounding material to produce plastic deformation and flow. When these hard particles were sliding on the wear surface, they suffered the effect of the load, increasing the stress and plastic flow around them, leading to the appearance of the fatigue crack. The fatigue crack developed during loading, and then a fine fatigue crack formed on the wear surface. With the rotation of the ceramic ball, the fatigue intensified and led to the material falling off from the wear surface.

2.4 Synergistic effect

Fig.7 shows the mechanistic map of the *AC-PA* (corrosion losses) for the alloy against the *PA* (mechanical losses), which could establish the balance between mechanical and corrosion degradation. Based on Eq.(3), the term *AC-PA* represents the corrosion contribution to synergy. In the region of (*AC-PA*)/*PA*=10, corrosion is dominant; if the (*AC-PA*)/*PA*=1, the regime is corrosion-abrasion; when the (*AC-PA*)/*PA*=0.1, the regime is abrasion-corrosion. The remaining region is mechanically dominated [23]. It is apparent that the data for the SiC F1200 and Al_2O_3 F1200 particles are in the corrosion-abrasion (*CA*) regime where the mechanical material losses are equal to or up to one times the corrosion losses. For the SiC F1000 and SiC F2000 particles, the data for the (*AC-PA*)/*PA* are in the abrasion-corrosion (*AC*) regime. It is interesting to note the data for the SiC F2000 and SiC F1000 particles are in the upper and lower bounds, respectively. This is likely due to the size of the abrasive particles, as shown in Table 2. For the SiC F1000 particle, the data for the (*AC-PA*)/*PA* are closer to the mechanical region, due to its larger size, and the data for SiC F2000 particle are closer to the corrosion-abrasion regime. These results indicate that the material loss caused by the larger sized particle is primarily due to mechanical destruction, that is the contribution of wear is bigger than the corrosion.

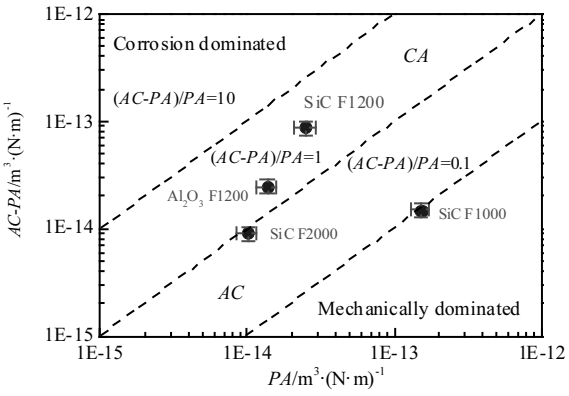

Fig.7 Mapping of *AC-PA* for the TLM alloy against *PA*

3 Conclusions

1) The specific wear rates increases as the particle size increases. For the same-sized particles, the material loss caused by the SiC F1200 is greater than that of the Al_2O_3 F1200 particle because the SiC particle has higher machinability.

2) For SiC particle, the average friction coefficients obtained in Hank's solution are larger than those in distilled water, while the opposite is true for the Al_2O_3 particle. For the same-sized particles, the average friction coefficients acquired by the Al_2O_3 particle is larger than by the SiC particle. In addition, the stability of the friction coefficient during the test in Hank's solution is poor compared with that in distilled water due to the corrosive nature of Hank's solution.

3) As the particle size decreases, the wear mechanism changes from three-body rolling wear to mixed mode (rolling and grooving wear) and finally to two-body grooving wear.

4) Through observation of the mechanistic map, the main regime is abrasion-corrosion, indicating that the contribution of the material loss from corrosion cannot be ignored.

References

1 Yu Z T, Zhou L. *Materials Science and Engineering A*[J], 2006, 438-440: 391

2 Paladugu M, Kent D, Wang G *et al*. *Materials Science and Engneering A*[J], 2010, 527: 6601

3 Yu S, Yu Z T, Wang G *et al*. *Colloids and Surfaces B: Biointerfaces*[J], 2011, 85: 103

4 Yu S, Yu Z T, Han J Y *et al*. *Transactions of Nonferrous Metals Society of China*[J], 2012, 22: 3046

5 Yu Zhentao, Zheng Yufeng, Niu Jinlong *et al*. *Transactions of Nonferrous Metals Society of China*[J], 2007, 17: s495

6 Huang R, Zhuang H Y, Han Y. *Materials Science and Engineering: C*[J], 2014, 35: 144

7 Meng Q K, Guo S, Liu Q *et al*. *Progress in Natural Science: Materials International*[J], 2014, 2: 157

8 Guo S, Meng Q K, Liao G Y *et al*. *Progress in Natural Science: Materials International*[J], 2013, 2: 174

9 Guo S, Chen B, Meng Q K *et al*. *Progress in Natural Science: Materials International*[J], 2013, 1: 1

10 Wang Z, Huang W, Meng X. *Materials Science and Technology*[J], 2015, 11: 1335

11 Wang Z, Huang W, Ma Y L. *Materials Science and Engineering: C*[J], 2014, 42: 211

12 Huang W J, Wang Z G, Liu C L *et al*. *Journal of Bio- and Tribo-Corrosion*[J], 2015, 1: 1

13 Wang Z G, Li Y, Huang W J *et al*. *Journal of the Mechanical Behavior of Biomedical Materials*[J], 2016, 63: 361

14 Wang Z G, Huang W J, Li Y *et al*. *Materials Science and Engineering C*[J], 2017, 76: 1094

15 Suner S, Bladen CL, Gowland N *et al*. *Wear*[J], 2014, 317: 163

16 Shipway P H, Hogg J J. *Wear*[J], 2007, 263: 887

17 Silva F J G, Casais R B, Martinho R P *et al*. *Wear*[J], 2011, 271: 2632

18 Sun D, Wharton J A, Wood R J K. *Tribology International*[J], 2009, 42: 1595

19 Andrade M F C, Martinho R P, Silva F J G *et al*. *Wear*[J], 2009, 267: 12

20 Thakare M R, Wharton J A, Wood R J K *et al*. *Wear*[J], 2012, 276-277: 16

21 Gomez V A O, MacêDo M C S D, Souza R M *et al*. *Wear*[J], 2015, 328-329: 563

22 Stack M M, Huang W, Wang G *et al*. *Tribology International*[J], 2011, 44: 1827

23 Telfer C G, Stack M M, Jana B D. *Tribology International*[J], 2012, 53: 35

24 Cozza R C. *Tribology International*[J], 2014,70: 52

25 Bello J O, Wood R J K, Wharton J A. *Wear*[J], 2007, 263: 149

26 Pang Y X, Huang W J, Tan Y Q *et al*. *Fundamental of Engineering Tribology*[M]. Beijing: China Coal Industry Publishing House, 2004: 39

27 Sasada T, Oike M, Emori N. *Wear*[J], 1984, 97: 291

28 Fowler G, Pashby I R, Shipway P H. *Wear*[J], 2009, 266: 613

29 Stachowiak G B, Salasi M, Rickard W D A *et al*. *Corrosion Science*[J], 2016, 111: 690

30 PeñA A, Gallardo E A, MoráN A *et al*. *Proceedings of the Institution of Mechanical Engineers J*[J], 2013, 5: 486

31 Costa H L, Ardila M A N, Labiapari W S *et al*. *Wear*[J], 2015, 324-325: 129
32 Pintaude G, Tanaka D K, Sinatora A. *Wear*[J], 2003, 255: 55
33 Stachowiak G B, Stachowiak G W, Brandt J M. *Tribology International*[J], 2006, 39: 1
34 Mezlini S, Zidi M, Arfa H, Tkaya M B *et al*. *Comptes Rendus Mécanique*[J], 2005, 11: 830
35 Cozza R C, Tanaka D K, Souza R M. *Wear*[J], 2009, 1-4: 61

SiC 和 Al_2O_3 颗粒对 Ti-25Nb-3Mo-3Zr-2Sn 合金微磨损行为的影响

王振国[1], 毕衍泽[1], 李 岩[1], 蔡海娇[2]

(1. 北京航空航天大学，北京 100191)
(2. 有研医疗器械（北京）有限公司, 北京 102200)

摘 要：研究了 SiC 和 Al_2O_3 颗粒对生物医用植入材料 Ti-25Nb-3Mo-3Zr-2Sn 合金的微磨损行为的影响。研究了合金的比磨损率、摩擦系数、磨损机制以及微磨损与腐蚀之间的协同作用。结果显示，合金的比磨损率随磨粒尺寸的增加而增加。由于 SiC 磨粒的硬度和切削性均优于 Al_2O_3 磨粒，由此在同尺寸磨粒下 SiC 磨粒所造成的材料的损失比 Al_2O_3 磨粒造成的要大。摩擦系数的结果显示，在同一种磨粒作用下，Hank's 溶液中所获得的摩擦系数的平均值大于蒸馏水中所获得的摩擦系数平均值，且由于 Hank's 溶液的腐蚀性所致在 Hank's 溶液中获得的摩擦系数的稳定性要比在蒸馏水中的稳定性差；在同尺寸磨粒下，Al_2O_3 磨粒所造成的摩擦系数要大于 SiC 磨粒。随磨粒尺寸的减小，磨损机制由三体磨损转变为混合磨损之后再转变为二体磨损。从磨损机制图中可以看出腐蚀对材料损失的贡献是不容小视的，磨损机制为以磨损为主的磨损腐蚀。

关键词：微磨损；磨粒；生物材料；Ti-25Nb-3Mo-3Zr-2Sn；协同作用

作者简介：王振国，男，1983 年生，博士，北京航空航天大学材料科学与工程学院，北京 100191，电话：010-82315989，E-mail: wzghappy@buaa.edu.cn